Investigation of Broadband Characteristics of Multi-Frequency Piezoelectric Micromachined Ultrasonic Transducer (MF-pMUT)

Changhe Sun, Qiongfeng Shi, Mahmut Sami Yazici, Takeshi Kobayashi, Yufei Liu, and Chengkuo Lee*, *Member, IEEE*

Abstract—**Multi-frequency ultrasonic transducers are highly promising devices in biomedical applications for providing both good imaging resolution and large detection depth. However, most conventional multi-frequency ultrasonic transducers are designed through integrating multiple single-frequency transducers, with complicated fabrication process, imperfect beam profiles and limited bandwidths. In this paper, a single-element multi-frequency piezoelectric micromachined ultrasonic transducer (MF-pMUT) is proposed and investigated in terms of broadband property. Three rectangular-diaphragm MF-pMUTs with different length-to-width aspect ratios are fabricated with the microelectromechanical system (MEMS) technology and characterized both in air and underwater. All MF-pMUT samples exhibit at least two broad bands. After optimization of the aspect ratio, two smooth bands with comparable sound pressure level are achieved, providing -6 dB bandwidths of 112% /38% and corresponding central frequencies of 0.615 MHz /1.63 MHz. Benefited from such broadened multi-frequency property and simple structure design, the proposed MF-pMUT shows a great potential in ultrasonic detection, diagnosis and imaging applications as well as wireless acoustic energy transmission.**

Index Terms—**Piezoelectric micromachined ultrasonic transducer (pMUT), microelectromechanical system (MEMS), mode merging, multi-frequency, large bandwidth**

I. INTRODUCTION

ULTRASOUND based medical imaging, detection and therapy have become an important and effective tool for applications ranging from clinical cardiology and obstetrics to remarkable human cancer treatments [1-3]. The conventional ultrasound generators based on piezoelectric or capacitive transducers usually can only work on one frequency band, which is generally at its fundamental mode. However, single-frequency ultrasound transducers typically suffer from a tradeoff between the deep penetration and high resolution. Although broadband ultrasound transducers have been widely studied to improve the imaging resolution without lessening the detection depth, it is still challengeable to design one single-frequency transducer with operation band covering both low frequency range of 0.5-3.5 MHz for high-intensity therapy and large detection distance, and high frequency range of 5-20 MHz for fine biomedical imaging resolution. Alternatively, multi-frequency ultrasound transducers (MFUTs) have recently received increasing attention due to several advantages, including the improved signal-to-noise ratio [4], enhanced acoustic cavitation effect [5], high imaging resolution [6], and multi-functional applications [7, 8].

There have been several attempts to realize multi-frequency ultrasound operation based on multi-element or single-element transducer array [9-20]. Generally, it is much easier to control desired frequency bands through multiple single-frequency transducers because of independent optimization for geometric structure. For example, a MFUT can be configured with several single-frequency transducers by using bulk piezoelectric ceramic pieces in series [9-11]. This design has poor beam alignment and compromised elevational focusing. One way to improve the beam profile is to interleave different elements within the shortest wavelength in the horizontal plane [12, 13]. However, a primary difficulty for this design is that all dimensions of different fabricated membranes must meet the lambda pitch requirement. Another way to ensure good beam profile is to stack different device layers in the normal plane [14-16], but a frequency selective isolation layer for the stacked scheme is usually needed to suppress the crosstalk between two stacked elements as an acoustic filer [17, 18], which unavoidably increases the complexities of the transducer design and microfabrication. For the case with single ultrasound transducer, the multi-band operation can also be achieved by exciting its fundamental and harmonic modes [19-21]. Due to the weak resonances and limited pressure sensitivity at higher-order modes, this multi-frequency operation relies highly on nonlinear contrast agent excitation. Although the multi-

C. Sun and Y. Liu are with the Key Laboratory of Optoelectronic Technology & Systems (Chongqing University), Ministry of Education, and Centre for Intelligent Sensing Technology, College of Optoelectronic Engineering, Chongqing University, Chongqing 400044, China. (e-mail: yufei.liu@cqu.edu.cn).

C. Sun, Q. Shi, M. S. Yazici and C. Lee are with the Department of Electrical and Computer Engineering, National University of Singapore, Singapore 117583 (e-mail: elecl@nus.edu.sg).

T. Kobayashi is with the National Institute of Advance Industrial Science and Technology (AIST), Tsukuba, Ibaraki 305-8564, Japan.

frequency mechanism can be realized by patterning the top electrodes into several segments and activating different modes via the electrically frequency switchable control circuit [22], the frequencies can only be generated within a narrow range and the interconnection for patterned electrodes needs to be taken into more consideration. The bandwidths for harmonics are also limited mainly due to small high-to-low modal frequency ratio, which is typically less than 3.5 and cannot meet high-resolution imaging requirements. Therefore, a simple and easy-to-fabricate multi-frequency ultrasound transducer with large bandwidth is highly preferred.

The reported MFUTs are mainly focused on piezoelectric micromachined ultrasonic transducers (pMUTs) and capacitive micromachined ultrasonic transducers (cMUTs). Although cMUTs can exhibit a wider bandwidth of over 130% compared with pMUTs [13], the ultrahigh bias voltage significantly restricts its biomedical applications due to the safety concerns. Furthermore, to obtain the acceptable sound pressure level (SPL), an extremely small capacitive cavity (typically < 200 nm) is required [23, 24], which requires highly complicated and precise fabrication process and degrades the device yield rate. The pMUTs with operation voltage of as low as only several volts, on the other hand, have excellent potential for practical medical diagnosis, therapy and imaging applications as well as portable electronics. One of the biggest challenges is its insufficient bandwidth due to the large acoustic impedance mismatch. To overcome this drawback, a broadband property can be achieved by applying and mixing multiple elements with different sizes [19], but the wide bandwidth is achieved from the whole array instead of an individual pixel. Another band broadening method was recently developed by our group. Through adjusting the length-to-width aspect ratio of a rectangular piezoelectric diaphragm to cover the first several adjacent modes within a narrow frequency range, a -6 dB bandwidth of 95% was achieved underwater [25]. However, the multi-frequency property for such rectangular piezoelectric diaphragm still has not been revealed and investigated yet. A more comprehensive study is required to demonstrate the difference and transition between vibration modes of the rectangular diaphragm and those of the square diaphragm.

Because of the Poisson coupling between the bending motions in the longitudinal and transverse directions, there are some degenerated flexural vibration modes for a square diaphragm. When the square diaphragm becomes rectangular, the degenerated two-dimensional modes would be split into two sets of pure non-degenerated string modes, whose nodal lines are parallel to the length and width. These new string modes redistribute and form multiple separated frequency ranges, each of which covers several resonant modes. Therefore, in this work, a simple and easy-to-fabricate multi-frequency pMUT (MF-pMUT) based on rectangular diaphragm is proposed and investigated in terms of the broadband property. By exciting the rectangular-shaped pMUT instead of square or circular pMUTs, the flexural vibration modes are asymmetrically redistributed in the modal spectrum and thus multiple separated frequency ranges are formed, producing multiple broad bands in a largely damped medium. Three MF-pMUT samples with different length-to-width aspect ratios are fabricated with the microelectromechanical system (MEMS) technology and characterized both in air and underwater, all showing at least

two broad bands. The proposed MF-pMUT shows great promise in ultrasonic detection, diagnosis and imaging applications.

II. DESIGN AND METHODS

A. Multi-band mechanism of rectangular MF-pMUT

In general, most flexural vibration modes dominating in the response spectrum of the square- or circular-diaphragm pMUTs are degenerated due to the highly symmetrical structure. These degenerated modes are spaced far away from each other and have very low output compared with that of the fundamental mode. However, when the piezoelectric diaphragm is designed into the rectangular shape with less symmetricity, the degenerated modes will be split into one pair of pure undegenerated string modes and redistributed in the spectrum. These new string modes with nodal lines parallel to the length and width can be adjusted by the length-to-width aspect ratio and gathered within a set of frequency ranges. The interaction and transition between mode shapes from square diaphragm to rectangular diaphragm can be explained in Fig. 1. It is worth mentioning that the degenerated modes through opposite combination would be missing in the response spectrum due to the cancellation of opposite motions.
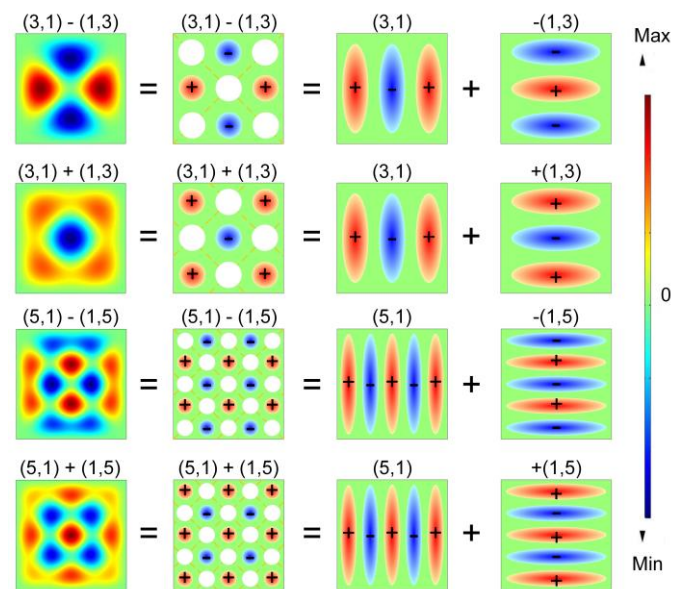

Fig. 1. Mode interaction and transition between square diaphragm and rectangular diaphragm

The schematic drawing of the proposed rectangular-diaphragm MF-pMUT element is illustrated in Fig. 2, including a released supporting silicon layer, a silicon oxide layer and a piezoelectric diaphragm sandwiched between two metal electrodes. Though a rectangular pMUT model has been proposed by Wang *et al.* to study the relationship between the vibration modes and aspect ratio [25], the given expression in their work is only suitable for the simply supported boundaries instead of fully clamped case which is much closer to the real boundary condition, resulting in a large calculation error in the high-order modes. Here, we rebuild the rectangular-diaphragm MF-pMUT model with the fully fixed edges. To simplify the calculation of modal frequencies, the MF-pMUT is considered

as a single-layer uniform rectangular diaphragm with dimensions L and W (The length-to-width aspect ratio is $R_{L/W} = L / W$). Based on the squared trigonometric functions to approximate the mode shapes [26], the modal frequencies can be derived by applying the Galerkin method:

$$f_{(m,n)} = \frac{2\pi}{3} \frac{\lambda_{(m,n)}}{L^2} \sqrt{\frac{D}{\sigma}} \qquad m,n = 1,2,3,\cdots\cdots \quad (1)$$

$$\lambda_{(m,n)} = \sqrt{3\frac{m^4}{R_{L/W}^4} + 2\frac{m^2}{R_{L/W}^2}n^2 + 3n^4} \quad (2)$$

where D is the flexural rigidity and can be calculated exactly for the multilayer laminated membranes [16], σ is mass density per unit area of the diaphragm, $\lambda_{(m,n)}$ is the frequency factor determined by the boundary conditions, m and n are the total number of the resonant peaks and anti-resonant troughs lying in the length and width directions, respectively.
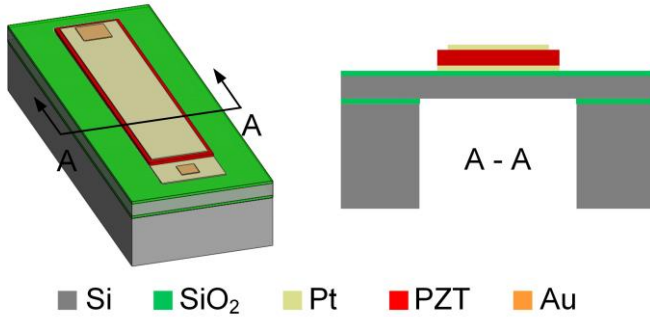

Fig. 2. Schematic drawing of the proposed rectangular-diaphragm MF-pMUT element.

When the aspect ratio $R_{L/W}$ is greater than 3, the frequencies will be dominated by the mode number n in the width direction, and the first $[nR_{L/W}]$ modes M(m, n) in the length direction will be compressed close to their corresponding first mode M(1, n). Then the frequency factor can be described

$$\lambda_{(m,n)} \approx \sqrt{2\frac{m^2}{R_{L/W}^2}n^2 + 3n^4}, \quad R_{L/W} \geq 3 \quad (3)$$

$$\lambda_{(m,n)} \rightarrow \sqrt{\frac{2n^2}{R_{L/W}^2} + 3n^4} \approx \lambda_{(1,n)}, \quad m \leq \left[nR_{L/W} \right] \quad (4)$$

Hence, due to the mode merging and synergistic effect when the MF-pMUT with a large aspect ratio operates in a largely damped medium, a set of frequency ranges will be formed in the response spectrum and each frequency range is centered around its first mode in the length theoretically. However, an optimization for the aspect ratio in the transducer design is necessary because the appropriate aspect ratio is helpful to gather more modes within each frequency range and benefits to broadband operation, while too large aspect ratio will in turn reduce the working bandwidth. The central frequency ratio (CFR) for the n-th and $1st$ frequency ranges can be approximately calculated by

$$CFR_{(n,1)} = \frac{f_{(1,n)}}{f_{(1,1)}} \approx n^2 \sqrt{\frac{3}{3 + 2/R_{L/W}^2 + 3/R_{L/W}^4}}, \quad n \geq 3 \quad (5)$$

For two specific bands, their CFR is only positively correlated with the aspect ratio $R_{L/W}$, demonstrating the effective controllability of the length-to-width aspect ratio to the high-to-low frequency ratio.

B. Device design and fabrication

To target the dual-frequency ultrasound operation centered at around 1 MHz and 5 MHz which are widely used in biomedical imaging [11, 13, 15, 17], three rectangular-diaphragm MF-pMUT array samples with length-to-width aspect ratios of 2, 4 and 6 have been micro-manufactured on a silicon-on-insulator (SOI) wafer with 10 μm device layer and 1 μm buried oxide (BOX) layer, as shown in Fig. 3(a). Each MF-pMUT array contains 11 or 14 elements in series. The dimensions of three MF-pMUT elements are 250 μm (W) ×500 μm (L), 250 μm (W) × 1000 μm (L) and 250 μm (W) × 1500 μm (L), respectively. The cross-sectional view and top view scanning electro-microscopy (SEM) images of three MF-pMUT samples are shown in Fig. 3(b)-(e).
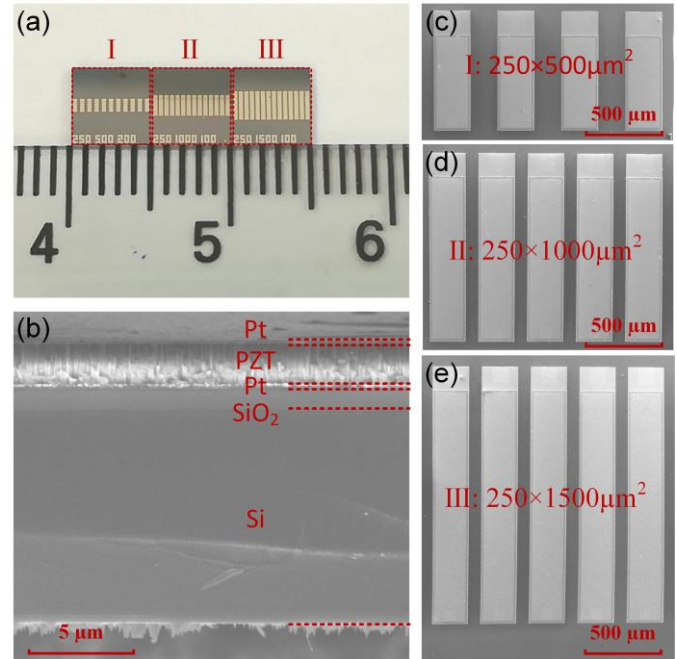

Fig. 3. (a) Photographs of three MF-pMUT arrays, (b) cross-sectional view and (c)-(e) top view SEM images of three MF-pMUT arrays.

The fabrication process flow of the MF-pMUTs is shown in Fig. 4 and the detailed steps are as follows. Firstly, a 1 μm SiO₂ layer is sputtered on the top surface of the SOI wafer. Then, 200 nm Pt/10 nm Ti thin metal layers are deposited as the bottom electrode (BE) by DC magnetron sputtering and a 1.9 μm piezoelectric PZT layer is formed using sol-gel process. After that, another 200 nm Pt/10 nm Ti thin metal layers are deposited and patterned as the top electrode (TE). To optimize the displacement sensitivity, a partially covered top-electrode with width of 220 μm is designed [27]. Lastly, the Si substrate and BOX layer are backside etched to release the diaphragm by deep reaction-ion etching (DRIE) process. In order to achieve a higher d_{31} coefficient, a unipolar pulse poling process is used after the device wire-bonding [28].
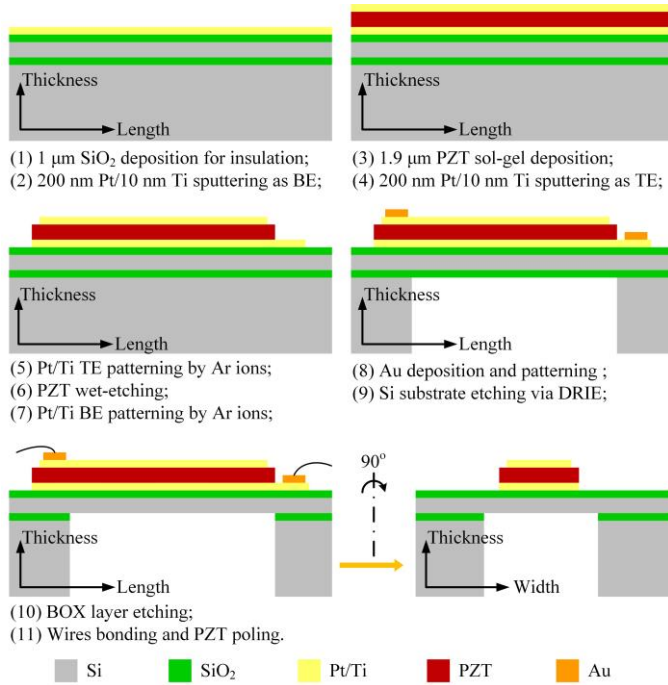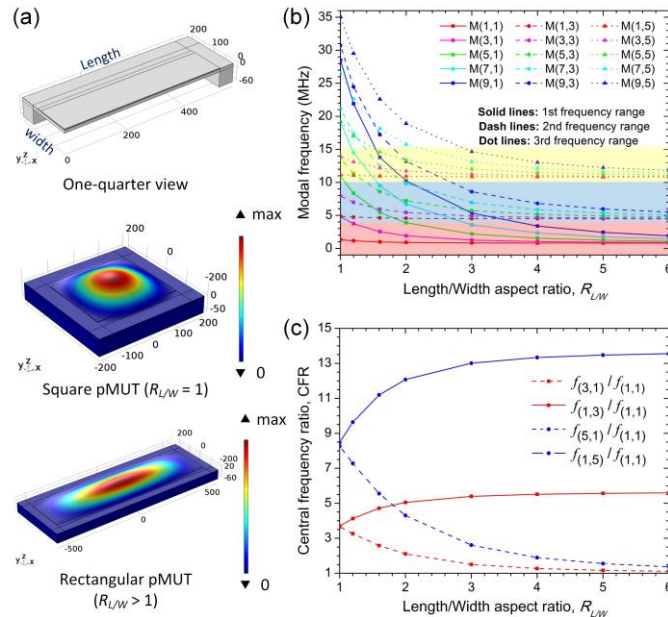
Fig. 4. Fabrication process flow of the MF-pMUT

Fig. 5. (a) FEM models of the square and rectangular pMUTs; (b) relationship between the modal frequencies and length-to-width aspect ratios; and (c) central frequency ratio varying with the aspect ratio.

TABLE I
MATERIAL PROPERTIES OF THE PMUT

Materials	Young's Modulus (GPa)	Poisson ratio	Mass density (kg/m^3)	d_{31} (pC/N)
Si	170	0.28	2329	/
SiO$_2$	70	0.17	2200	/
PZT	81.3	0.329	7500	-123
Pt	168	0.38	21450	/

C. FEM simulations

3-D finite-element method (FEM) models of the square and rectangular pMUTs with different aspect ratios were created using COMSOL Multiphysics v5.2a software to study their frequency properties, as shown in Fig. 5(a). The width of all pMUTs is kept at 250 μm. Material properties used for pMUT simulations are listed in Table I. The relationship between modal frequencies and aspect ratios is shown in Fig. 5(b). As is aforementioned, with increasing the length-to-width aspect ratio, three frequency ranges are formed and gathered at the first three odd modes M(1, n) (n = 1, 3, 5) in the width direction. The central frequency ratio (CFR) varying with the aspect ratio is shown in Fig. 5(c). When the aspect ratio rises from 1 (square diaphragm), the central frequency ratio $CFR_{(3,1)}$ for the first two frequency ranges increases from 3.6 to over 5.6 according to simulations. Therefore, one advantage of the proposed MF-pMUT is that the CFR for two bands can be changed by adjusting the aspect ratio, which is much more advantageous than the conventional transducers with only one fixed frequency ratio.
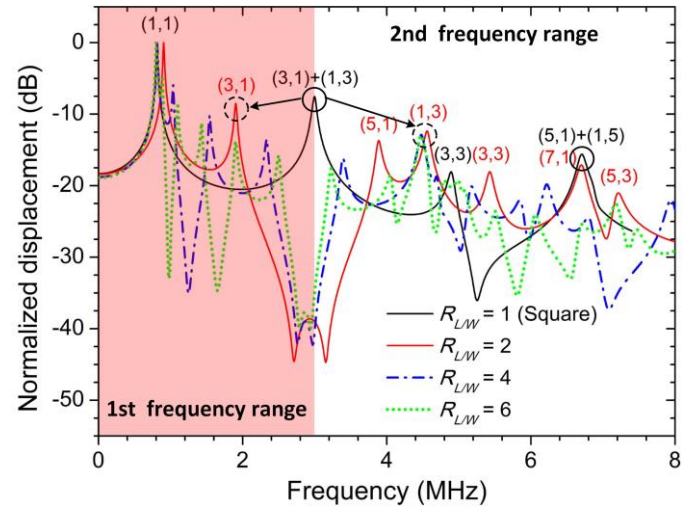

Fig. 6. Simulated response spectra of MF-pMUTs with different length-to-width aspect ratios.

The displacement-frequency spectra of the MF-pMUTs with different length-to-width aspect ratios were also simulated at the central point of the piezoelectric membrane and shown in Fig. 6. The degenerated modes of the conventional square pMUT are split into two parts, one of which approaches to the fundamental mode (1,1) while the other is kept at a higher frequency value as the aspect ratio increases. Due to the mode redistribution through adjusting the aspect ratio, two narrow frequency ranges are formed and each of them covers several flexural vibration modes. Hence, it is promising to achieve a broad band through the mode merging in damped medium for each frequency range. It is noted that the even modes are missing in the response spectrum because of the cancellation of opposite propagating motions [25, 29].

III. RESULTS AND DISCUSSIONS

A. In-air characterization

To characterize the frequency-related performance of the MF-pMUTs, three microfabricated samples are firstly

measured under 1 Vpp voltage excitation using DHM-R2100 holographic MEMS motional analyzer by Lyncée Tec. Ltd, as shown in Fig. 7(a)-(c). Compared with the COMSOL simulation results, all odd modes in the length and width directions are similarly excited. Besides, some even modes which should not appear ideally were also captured in the experiments. This may be caused by the asymmetrically distributed residual stress during the fabrication and polarization. Fortunately, these even modes integrated in the odd modes are beneficial to the broadband operation. It is noticed that all frequencies of three samples are slightly lower than simulations because of the deviation of dimensions, the residual stress and the air damping of the multilayer membranes. Furthermore, the edge-clamped boundary condition of the supporting layers in the simulation model does not precisely represent the dynamics of the fabricated MF-pMUT, which will result in a slight increase in the resonance frequencies. However, for the displacement amplitude, there is a large difference between the experiments and simulations because of the residual stress and air damping. This negative influence on the displacement gets much more significant when the rectangular membrane becomes larger, i.e., the length-to-width aspect ratio is larger. On the contrary, the simulated displacement would increase with the aspect ratio due to the larger area to perimeter ratio and resultant softened spring constant, as shown in Fig. 7(d).
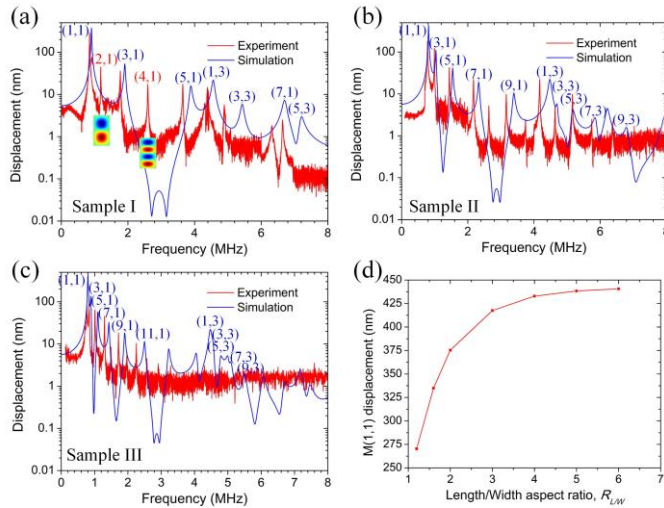

Fig. 7. Measured and simulated frequency-swept displacement response of three MF-pMUTs: (a) Sample I 250 × 500 μm², (b) Sample II 250 × 1000 μm² and (c) Sample III 250 × 1500 μm²; (d) simulated displacement varying with the aspect ratios.

Electrical impedance characterization was also carried out using Agilent 4294A precision impedance analyzer to determine the resonant frequencies and the electromechanical coupling coefficients of three MF-pMUT samples with different aspect ratios. The measured frequency-swept impedance and phase are shown in Fig. 8. It is clearly seen that there are two wide frequency ranges covering 0.8 ~ 3.6 MHz low frequencies (Fig. 8(a), (c) and (e)) and 4.3 ~ 6.8 MHz high frequencies (Fig. 8(b), 4(d) and 4(f)), which are consistent with the above displacement-based results. However, owing to very low self-resonance frequencies (< 11 MHz) of all samples, only the first two frequency ranges can be observed. The

electromechanical coupling coefficient is defined by resonance frequency and anti-resonance frequency, according to Eq. (6) [30]. Therefore, the in-air electromechanical coupling coefficients of three samples can be calculated, as shown in the Table II.

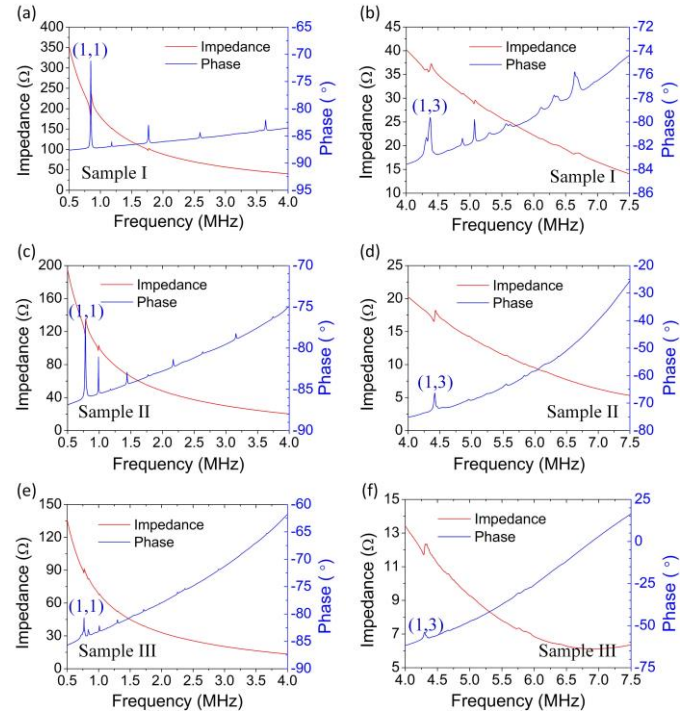$$k_{eff}^2 = \frac{f_a^2 - f_r^2}{f_a^2} \qquad (6)$$

Fig. 8. Measured impedance and phase for three MF-pMUT samples: (a) low frequency range and (b) high frequency range of Sample I with the aspect ratio of 2, (c) low frequency range and (d) high frequency range of Sample II with the aspect ratio of 4, (e) low frequency range and (f) high frequency range of Sample III with the aspect ratio of 6.

TABLE II
IN-AIR ELECTROMECHANICAL COUPLING COEFFICIENTS OF MF-pMUT SAMPLES WITH THE ASPECT RATIOS OF 2, 4 AND 6

k_{eff}^2	Sample I	Sample II	Sample III
Mode (1,1)	3.26%	3.01%	1.52%
Mode (3,1)	1.15%	1.61%	1.46%
Mode (5,1)	0.86%	1.11%	1.47%
Mode (1,3)	1.94%	1.19%	1.36%
Mode (3,3)	0.66%	0.98%	0.81%

B. Underwater characterization

To further evaluate the acoustic performance of the rectangular-diaphragm MF-pMUTs, an underwater ultrasound transmitting testing setup is established. The experimental configuration is shown in Fig. 9, where the designed MF-pMUT element is connected to a high-frequency Agilent 81150A pulse generator and driven by a 4 V$_{pp}$ electrical pulse signal. A needle hydrophone calibrated up to 20 MHz with 8 dB pre-amplifier and DC coupler (1.0 mm, SN2118, Precision Acoustic Ltd., UK) is utilized to receive the generated ultrasound signals at about 5 mm distance. The Agilent MSO-X 4104A mixed signal

oscilloscope is used to display and FFT transfer the received time-domain signals. Duration of the exciting pulse is 100 ns.
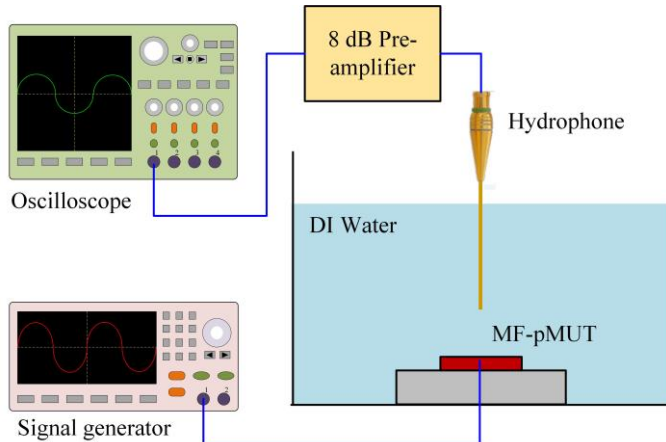

Fig. 9. Testing setup for underwater acoustic experiment.

The received signals are shown in Fig. 10(a)-(c). Though there are some fluctuations within each frequency band due to low noise-to-signal ratio, it is clearly shown that there are at least two frequency bands for all samples, corresponding to the first two frequency ranges as predicted in the analytical model (Fig. 5 and 6). Among three rectangular MF-pMUT samples, Sample I with a small aspect ratio shows -6 dB bandwidths of 118% for the first band with central frequency of 0.685 MHz, 36% for the second band with central frequency of 1.415 MHz, and 18% for the third band with central frequency of 2.095 MHz. However, due to the large modal frequency spacing and imperfect mode merging between the first two odd modes (1,1) and (3,1), there are two remarkable ripples beyond -4 dB in the passband. Sample II with a medium aspect ratio, which similarly shows two large -6 dB bandwidths of 112% and 38%, however, has a much smoother passband because of good overlapping of at least the first three odd modes. The central frequencies of the first two bands for Sample II are 0.615 MHz and 1.63 MHz, respectively. With the length-to-width aspect ratio continuously increasing, Sample III exhibits a greatly compromised -6 dB bandwidth owing to the over-compression for the modes merged within each band. For the comparison, the frequency bandwidths of previously reported MFUTs are summarized in Table III. Therefore, from the perspective of device design and working bandwidth, the rectangular-diaphragm MF-pMUT is much superior to the conventional multi-frequency piezoelectric transducers. When the designed MF-pMUT is used for imaging applications, some filters aimed at different bands could be employed through an electrically switchable filter circuit to further improve the axis resolution.

TABLE III
FREQUENCY BANDWIDTHS OF PREVIOUSLY REPORTED MULTI-FREQUENCY ULTRASOUND TRANSDUCERS

Device Type	1st Band	2nd Band	Ref.
Multiple bulk transducers	18%	67%	[11]
Multiple pMUTs	37%	23%	[15]
Multiple pMUTs	-	52%	[17]
Multiple pMUTs	55%	34%	[19]
Multiple cMUTs	130%	90%	[13]

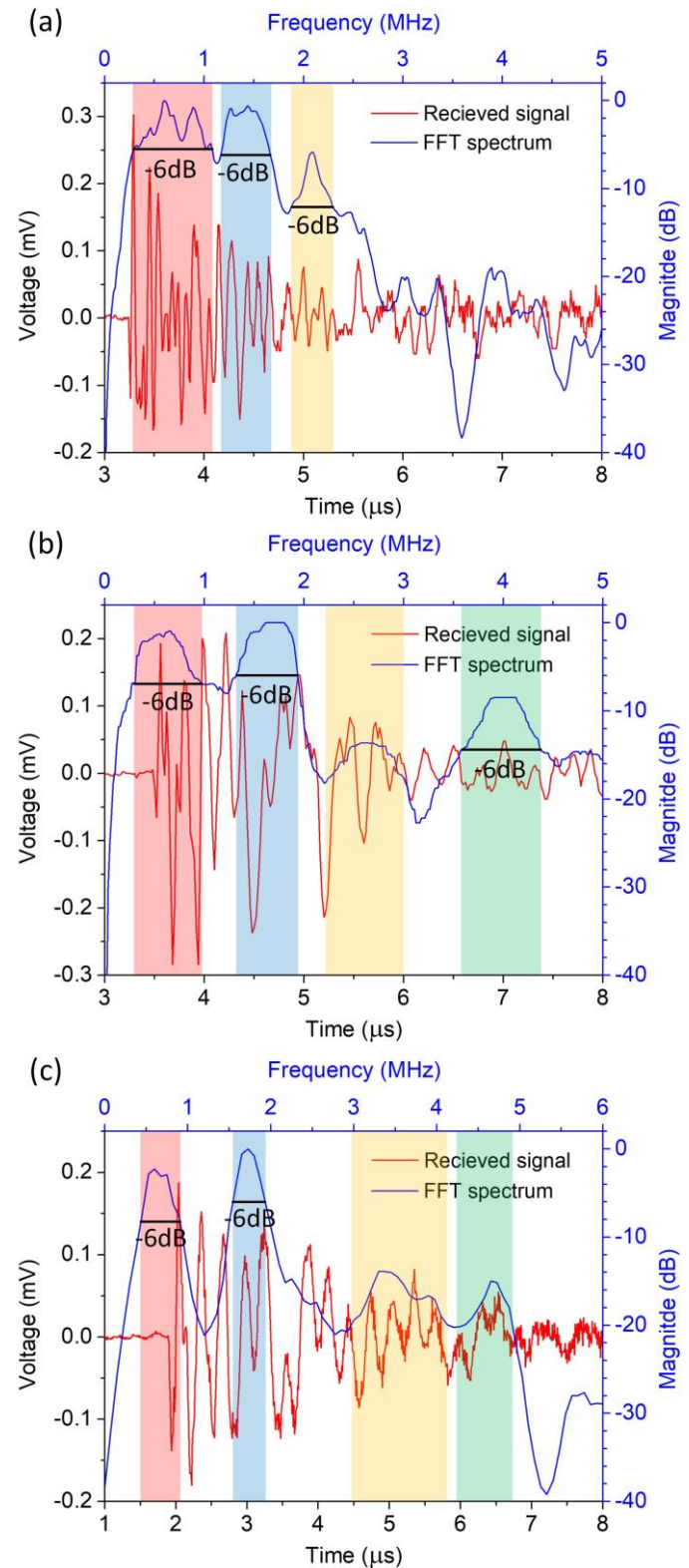|			
Single pMUT	118%	36%	Sample I
Single pMUT	112%	38%	Sample II
Single pMUT	70%	22%	Sample III

Fig. 10. (a)-(c) Received time-domain acoustic pulses and their FFT spectra measured at 5 mm depth by hydrophone. MF-pMUT samples are excited by 100 ns pulse signals with amplitude of 4 V_{pp}.

IV. Conclusion

In summary, a broadband and multi-frequency operation is obtained using the single-element rectangular-diaphragm MF-pMUT without complicated fabrication processes and matching layers. Three MF-pMUT samples with different length-to-width aspect ratios are fabricated and characterized both in air and underwater. Configured with a small aspect ratio, the MF-pMUT exhibits two wide bands while its first band suffers from several fluctuations due to the imperfect mode merging. On the other hand, a better multi-frequency and broadband ultrasound operation can be achieved when the MF-pMUT is designed with a medium aspect ratio. Two smooth bands with the -6 dB bandwidths of 112% and 38% are obtained in this work, which are significantly larger than those of previously reported multi-frequency piezoelectric transducers. Because of the very simple design and advantageous behaviors, the rectangular-diaphragm MF-pMUTs promisingly facilitate diversified ultrasound applications, especially in modern medical detection, imaging and therapy.

References

[1] M. Cikes, L. Tong, G. R. Sutherland, and D'Hooge, "Ultrafast cardiac ultrasound imaging: technical principles, applications, and clinical benefits," *Jacc Cardiovasc Imag.*, vol. 7, no. 8, pp. 812-823, 2014.

[2] B. R. Benacerraf *et al.*, "Three- and 4-Dimensional Ultrasound in Obstetrics and Gynecology," *J. Ultrasound Med.*, vol. 24, no. 12, pp. 1587-97, 2005.

[3] B. D. Lindsey, J. Kim, P. A. Dayton, and X. Jiang, "Dual-Frequency Piezoelectric Endoscopic Transducer for Imaging Vascular Invasion in Pancreatic Cancer," *IEEE Trans. Ultrason. Ferroelectr. Freq. Control*, vol. PP, no. 99, pp. 1-1, 2017.

[4] A. Bouakaz, B. J. Krenning, W. B. Vletter, F. J. ten Cate, and J. N. De, "Contrast superharmonic imaging: a feasibility study," *Ultrasound Med. Biol.*, vol. 29, no. 4, pp. 547-553, 2003.

[5] H. L. Liu and C. M. Hsieh, "Single-transducer dual-frequency ultrasound generation to enhance acoustic cavitation," *Ultrason. Sonochem.*, vol. 16, no. 3, pp. 431-438, 2009.

[6] T. Ma, M. Yu, Z. Chen, C. Fei, K. K. Shung, and Q. Zhou, "Multi-Frequency Intravascular Ultrasound (IVUS) Imaging," *IEEE Trans. Ultrason. Ferroelectr. Freq. Control*, vol. 62, no. 3, pp. 604-604, 2015.

[7] J. P. Kilroy, J. A. Hossack, A. L. Klibanov, and B. R. Wamhoff, "Multifunction intravascular ultrasound for microbubble based drug delivery," in *Proc. IEEE Int. Ultrason. Symp. (IUS)*, 2013, pp. 2168-2171.

[8] X. Qian, M. Teng, M. Yu, X. Chen, K. K. Shung, and Q. Zhou, "Multi-functional Ultrasonic Micro-elastography Imaging System," *Sci. Rep.*, vol. 7, no. 1, 2017.

[9] D. N. Stephens, D. E. Kruse, A. S. Ergun, S. Barnes, X. M. Lu, and K. W. Ferrara, "Efficient array design for sonotherapy," *Phys. Med. Biol.*, vol. 53, no. 14, p. 3943, 2008.

[10] R. Gessner, M. Lukacs, M. Lee, E. Cherin, F. S. Foster, and P. A. Dayton, "High-resolution, high-contrast ultrasound imaging using a prototype dual-frequency transducer: in vitro and in vivo studies," *IEEE Trans. Ultrason. Ferroelectr. Freq. Control*, vol. 57, no. 8, pp. 1772-1781, 2010.

[11] A. Guiroy *et al.*, "Dual-frequency transducer for nonlinear contrast agent imaging," *IEEE Trans. Ultrason. Ferroelectr. Freq. Control*, vol. 60, no. 12, pp. 2634-2644, 2013.

[12] C. H. Tsai, J. W. Zhang, Y. Y. Liao, and H. L. Liu, "Real-time monitoring of focused ultrasound blood-brain barrier opening via subharmonic acoustic emission detection: implementation of confocal dual-frequency piezoelectric transducers," *Phys. Med. Biol.*, vol. 61, no. 7, pp. 2926-2946, 2016.

[13] R. K. Chee, P. Zhang, M. Maadi, and R. J. Zemp, "Multi-Frequency Interlaced CMUTs for Photoacoustic Imaging," *IEEE Trans. Ultrason. Ferroelectr. Freq. Control*, vol. 64, no. 2, pp. 391-401, 2017.

[14] J. H. Sung and J. S. Jeong, "High-frequency ultrasound transducer by using inversion layer technique for intravascular ultrasound imaging," *Electron. Lett.*, vol. 52, no. 12, pp. 1003-1005, 2016.

[15] Z. Wang, K. H. Martin, W. Huang, P. A. Dayton, and X. Jiang, "Contrast Enhanced Superharmonic Imaging for Acoustic Angiography Using Reduced Form-factor Lateral Mode Transmitters for Intravascular and Intracavity Applications," *IEEE Trans. Ultrason. Ferroelectr. Freq. Control*, vol. 64, no. 2, pp. 311-319, 2017.

[16] C. Sun, S. Jiang, and Y. Liu, "Numerical Study and Optimisation of a Novel Single-Element Dual-Frequency Ultrasound Transducer," *Sensors*, vol. 18, no. 3, p. 703, 2018.

[17] T. Azuma, M. Ogihara, J. Kubota, A. Sasaki, S. Umemura, and H. Furuhata, "Dual-frequency ultrasound imaging and therapeutic bilaminar array using frequency selective isolation layer," *IEEE Trans. Ultrason. Ferroelectr. Freq. Control*, vol. 57, no. 5, p. 1211, 2010.

[18] J. Ma *et al.*, "Design factors of intravascular dual frequency transducers for super-harmonic contrast imaging and acoustic angiography," *Phys. Med. Biol.*, vol. 60, no. 9, pp. 3441-3457, 2015.

[19] A. Hajati *et al.*, "Three-dimensional micro electromechanical system piezoelectric ultrasound transducer," *Appl. Phys. Lett.*, vol. 101, no. 25, pp. 44-54, 2012.

[20] T. Hedegaard, T. Pedersen, E. V. Thomsen, R. Lou-Moeller, K. Hansen, and T. Zawada, "Screen printed thick film based pMUT arrays," in *Proc. IEEE Int. Ultrason. Symp. (IUS)*, 2009, pp. 2126-2129.

[21] H. H. Kim, J. M. Cannata, R. Liu, and C. Jin, "20 MHz/40 MHz dual element transducers for high frequency harmonic imaging," *IEEE Trans. Ultrason. Ferroelectr. Freq. Control*, vol. 55, no. 12, pp. 2683-2691, 2008.

[22] T. Wang and C. Lee, "Electrically switchable multi-frequency piezoelectric micromachined ultrasonic transducer (pMUT)," in *Proc. IEEE Int. Conf. Micro Electro Mech. Syst. (MEMS)*, 2016, pp. 1106-1109.

[23] Y. Lu, A. Heidari, and D. A. Horsley, "A High Fill-Factor Annular Array of High Frequency Piezoelectric Micromachined Ultrasonic Transducers," *J. Microelectromech. Syst.,* vol. 24, no. 4, pp. 904-913, 2015.

This article has been accepted for publication in a future issue of this journal, but has not been fully edited. Content may change prior to final publication. Citation information: DOI 10.1109/JSEN.2018.2878785, IEEE Sensors Journal

> REPLACE THIS LINE WITH YOUR PAPER IDENTIFICATION NUMBER (DOUBLE-CLICK HERE TO EDIT) <   8

[24] J. Duehansen *et al.*, "Fabrication process for CMUT arrays with polysilicon electrodes, nanometre precision cavity gaps and through-silicon vias," *J. Micromech. Microeng.*, vol. 22, no. 22, pp. 74009-74016(8), 2012.

[25] T. Wang, T. Kobayashi, and C. Lee, "Micromachined piezoelectric ultrasonic transducer with ultra-wide frequency bandwidth," *Appl. Phys. Lett.*, vol. 106, no. 1, p. 054004, 2015.

[26] A. Leissa, *Vibration of Plates*. Washington, DC, USA: Government Press, 1969.

[27] T. Wang, T. Kobayashi, B. Yang, H. Wang, and C. Lee, "Highly sensitive piezoelectric micromachined ultrasonic transducer (pMUT) operated in air," in *Proc. IEEE Int. Conf. Nano/micro Eng. Mol. Syst. (NEMS)*, 2016, pp. 294-299.

[28] T. Kobayashi, Y. Suzuki, N. Makimoto, H. Funakubo, and R. Maeda, "Influence of pulse poling on the piezoelectric property of Pb(Zr0.52,Ti0.48)O3 thin films," *AIP Advances*, vol. 4, no. 11, pp. 2431-33, 2014.

[29] Q. Shi, T. Wang, T. Kobayashi, and C. Lee, "Investigation of geometric design in piezoelectric microelectromechanical systems diaphragms for ultrasonic energy harvesting," *Appl. Phys. Lett.*, vol. 108, no. 19, p. 193902, 2016.

[30] J. Jung *et al.*, "31-mode piezoelectric micromachined ultrasonic transducer with PZT thick film by granule spraying in vacuum process," *Appl. Phys. Lett.*, vol. 110, no. 21, p. 744, 2017.

Changhe Sun received the B.Eng. degree from College of Optoelectronic Engineering at Chongqing University, China, in 2014. He is currently pursuing his Ph.D. in Instrument Science and Technology with Chongqing University, China. From 2017 to 2018, he was a visiting Ph.D. student in the Department of Electrical and Computer Engineering at National University of Singapore. His research interests focus mainly on ultrasonic transducers, MEMS resonant sensors and their applications.

Qiongfeng Shi received his B.Eng. degree from Department of Electronic Engineering and Information Science at University of Science and Technology of China in 2012 and Ph.D. degree from Department of Electrical and Computer Engineering at National University of Singapore in 2018. He is currently a Research Fellow in Dept. of ECE, NUS. His research interests are focused on energy harvesters and self-powered sensors.

Mahmut Sami Yazici received his B.S. degree in Electrical and Electronics Engineering and B.S. degree in Physics both from Bogazici University, Istanbul/Turkey, in 2017. Currently, he is pursuing his Ph.D. in the Electrical and Computer Engineering Department at NUS. His main research focus is MEMS based IR sensors.

Takeshi Kobayashi received his B.S. and M.S. degree in Materials Science from the University of Tokyo. He also received Ph.D. degree in Materials Science from the University of Tokyo in 2002. He worked as researcher in National Institute of Advance Industrial Science and Technology (AIST), Japan. His research interest includes piezoelectric MEMS devices and their application to wireless sensor network. He has contributed to more than 40 international journal papers and 40 conference proceedings. Two of his recent publications have been selected as highlighted paper of Journal of Micromechanics and Microengineering in 2007 and 2008

Yufei Liu received B.S. degree in Physics and B.A. in Economics in 2003 from Peking University, the M.Eng. degree in Microelectronics and Solid State Electronics in 2006 from Shanghai Institute of Microsystem and Information Technology, Chinese Academy of Science, and Ph.D. degree in 2011 from Heriot-Watt University. He is currently a Professor and Director of the Centre for Intelligent Sensing Technology, College of Optoelectronic Engineering, Chongqing University and his research interests are advance micro/nano fabrication, MEMS technology, and multifunctional microsystem for precision biomedical application.

Chengkuo Lee (S'93–M'96) received the M.S. degree in materials science and engineering from National Tsing Hua University, Hsinchu, Taiwan, in 1991, the M.S. degree in industrial and system engineering from Rutgers University, New Brunswick, NJ, in 1993, and the Ph.D. degree in precision engineering from The University of Tokyo, Tokyo, Japan, in 1996. He was a Foreign Researcher with the Nanometer Scale Manufacturing Science Laboratory, Research Center for Advanced Science and Technology, The University of Tokyo, from 1993 to 1996. He was with the Mechanical Engineering Laboratory, AIST, MITI, Japan, as a JST Research Fellow, in 1996. Thereafter, he became a Senior Research Staff Member with the Microsystems Laboratory, Industrial Technology Research Institute, Hsinchu. In 1997, he joined Metrodyne Microsystem Corporation, Hsinchu, and established the MEMS Device Division and the first micromachining fab for commercial purposes in Taiwan. He was the Manager of the MEMS Device Division from 1997 to 2000. He was an Adjunct Assistant Professor with the Electro-Physics Department, National Chiao Tung University, Hsinchu, in 1998, and the Institute of Precision Engineering, National Chung Hsing University, Taichung, Taiwan, from 2001 to 2005. In 2001, he co-founded Asia Pacific Microsystems, Inc., where he first became the Vice President of Research and Development, before becoming the Vice President of the Optical Communication Business Unit and a Special Assistant to the Chief Executive Officer in charge of international business and technical marketing for the microelectromechanical systems (MEMS) foundry service. From 2006 to 2009, he was a Senior Member of the Technical Staff with the Institute of Microelectronics, A*STAR, Singapore. He is currently an Associate Professor with the Department of Electrical and Computer Engineering, National University of Singapore, Singapore. He has co-authored the books Advanced MEMS Packaging (McGraw-Hill, 2010) and Micro and Nano Energy Harvesting Technologies (Artech House, 2014). He has contributed to more than 270 international conference papers and extended abstracts, and 300 peer-reviewed international journal articles in the fields of sensors, actuators, energy harvesting, MEMS, nanoelectromechanical systems, metamaterials, nanophotonics, and nanotechnology. He holds nine U.S. patents.